JACS
JOURNAL OF THE AMERICAN CHEMICAL SOCIETY
pubs.acs.org/JACS
Article

Stimuli-Modulated Metal Oxidation States in Photochromic MOFs

Corey R. Martin, Kyoung Chul Park, Gabrielle A. Leith, Jierui Yu, Abhijai Mathur, Gina R. Wilson, Gayathri B. Gange, Emily L. Barth, Richard T. Ly, Olivia M. Manley, Kelly L. Forrester, Stavros G. Karakalos, Mark D. Smith, Thomas M. Makris, Aaron K. Vannucci, Dmitry V. Peryshkov, and Natalia B. Shustova*

Cite This: J. Am. Chem. Soc. 2022, 144, 4457−4468

ABSTRACT: Tuning metal oxidation states in metal−organic framework (MOF) nodes by switching between two discrete linker photoisomers via an external stimulus was probed for the first time. On the examples of three novel photochromic copper-based frameworks, we demonstrated the capability of switching between +2 and +1 oxidation states, on demand. In addition to crystallographic methods used for material characterization, the role of the photochromic moieties for tuning the oxidation state was probed via conductivity measurements, cyclic voltammetry, and electron paramagnetic resonance, X-ray photoelectron, and diffuse reflectance spectroscopies. We confirmed the reversible photoswitching activity including photoisomerization rate determination of spiropyran- and diarylethene-containing linkers in extended frameworks, resulting in changes in metal oxidation states as a function of alternating excitation wavelengths. To elucidate the switching process between two states, the photoisomerization quantum yield of photochromic MOFs was determined for the first time. Overall, the introduced noninvasive concept of metal oxidation state modulation on the examples of stimuli-responsive MOFs foreshadows a new pathway for alternation of material properties toward targeted applications.

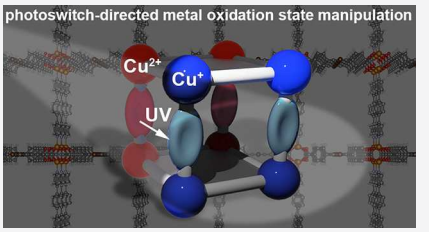

INTRODUCTION

Metal oxidation state modulation is paramount for tailoring and tuning the properties of materials (e.g., catalytic activity, stability, or charge/energy transport) and, therefore, defines their practical implementation.[1−11] For example, transition-metal-based catalysis almost exclusively relies on changes in the metal oxidation states during their catalytic cycles.[12−15] In a similar vein, mixed-valence metals determine the electronic properties of countless semiconducting materials.[16−26] Reversible tuning of metal oxidation states allows for switching between discrete states and is a key aspect for developing logic gates, spatially and temporally resolved sensors, and on-demand drug delivery systems.[27−30] These cutting-edge concepts could be realized, for instance, using an external stimulus (e.g., temperature, pressure, light, or pH).[31−38]

In the presented studies, we offer the realization of noninvasive oxidation state modulation through the integration of photoresponsive moieties inside novel copper-containing metal−organic frameworks (MOFs).[39−44] This approach provides an opportunity to control metal oxidation states as a function of an excitation wavelength (Scheme 1). In particular, we demonstrate the first example of metal oxidation state reversibility in novel two- and three-dimensional copper-based photochromic MOFs through light-induced transformations of two distinct classes of photoresponsive molecules. Fundamental insights into the frameworks' photophysical profiles and electronic structures are discussed extensively, including determination of photoisomerization rates ($k_{forward}$ and $k_{reverse}$) for novel copper-based photochromic MOFs. Cycling of optical and electronic response as a function of an excitation wavelength in photoresponsive frameworks was probed through diffuse reflectance (DR) spectroscopy and conductivity measurements. Electron paramagnetic resonance (EPR) and X-ray photoelectron spectroscopies (XPS) were used to monitor the photoinduced changes in oxidation states in the prepared MOFs under *in situ* and *ex situ* UV irradiation (λ_{ex} = 365 nm). Material structure and integrity were studied after linker photoisomerization in the MOFs by single-crystal and powder X-ray diffraction (PXRD), respectively. Finally, to shed light on the possible mechanism of modulating metal oxidation states, we estimated the photoisomerization quantum yield of photoresponsive moieties integrated within a rigid MOF matrix for the first time.

RESULTS AND DISCUSSION

As a "knob" for tuning metal oxidation states in MOFs, we chose two classes of distinct photochromic compounds,

Received: November 12, 2021
Published: February 9, 2022

https://doi.org/10.1021/jacs.1c11984
J. Am. Chem. Soc. 2022, 144, 4457−4468

Scheme 1. Photoswitch-Directed Oxidation State Modulation in Photochromic MOFs Is Brought into the Spotlight[a]

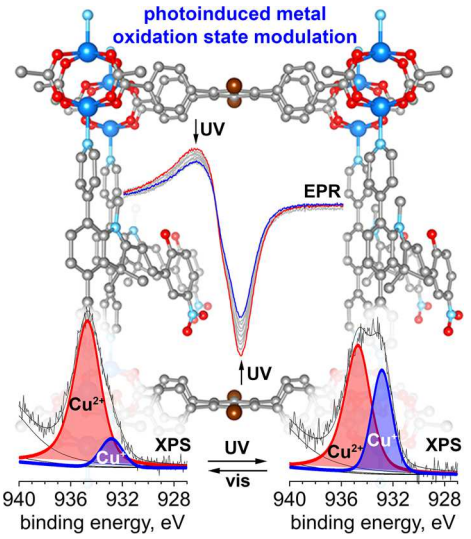

[a]Changes in EPR and XPS spectra were monitored as a function of an excitation wavelength. The gray, red, aqua, brown, and blue spheres represent C, O, N, Br, and Cu atoms, respectively.

diarylethene and spiropyran derivatives, based on the following aspects: (i) the possibility of linker integration inside an extended structure with preservation of the linker photochromic behavior;[41] (ii) the opportunity to probe the effect of the presence of a radical upon photoexcitation as a result of charge transfer;[42] and (iii) a wide range of photoisomerization rates due to distinct photoisomerization mechanisms.[45]

MOF Synthesis and Characterization. Spiropyran-containing compounds exhibit relatively fast photoisomerization in solution or in porous media[45] in comparison with diarylethene derivatives.[45] In the case of spiropyran derivatives, photoisomerization occurs due to an excited state heterocyclic bond cleavage of benzopyran to a metastable *cis*-merocyanine isomer and a subsequent *cis*-to-*trans* isomerization to form the zwitterionic merocyanine photoisomer (Figure 1).[31] In contrast, diarylethene and its derivatives undergo fast photoisomerization in the solid state due to minimal geometric reorganization required for switching between two photoisomers (Figure 1).[45−47] In particular, diarylethene undergoes a 6π-electron electrocyclic rearrangement, resulting in bond formation between the two methyl thiophene groups and extension of π-electron conjugation along the backbone, forming the colored photoisomer.[48]

For coordinative immobilization inside a framework, we prepared two diarylethene-based derivatives, 1,2-bis(2-methyl-5-(pyridin-4-yl)thiophen-3-yl)cyclopent-1-ene (BPMTC, Figure 1) and 4,4′-(cyclopent-1-ene-1,2-diyl)bis(5-methylthiophene-2-carboxylic acid) (H_2BCMTC, Figure 1),[49,50] as well as a spiropyran-based derivative, 1′,3′,3′-trimethyl-6-nitro-4′,7′-di(pyridin-4-yl)spiro[chromene-2,2′-indoline] (TNDS, Figure 1).[45] For control experiments, we selected 2,5-di(pyridin-4-yl)benzaldehyde (DPB-CHO, Figure S1)[51] as a non-photochromic analogue due to its applicability for preparation of isostructural MOFs for direct comparison of the structures containing photoresponsive diarylethene and spiropyran units.

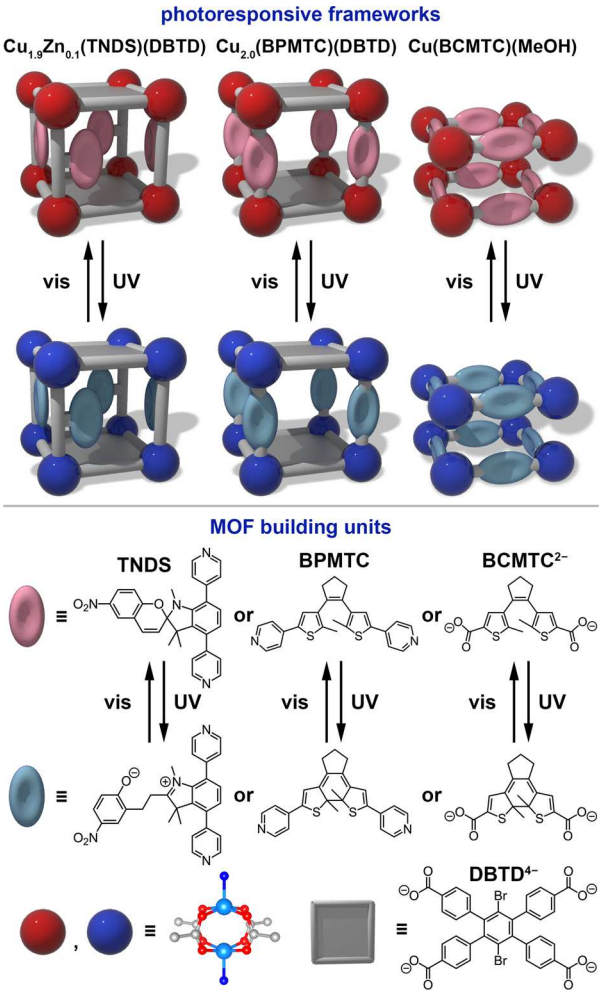

Figure 1. (Top) Schematic representation of photochromic MOFs prepared in the current work. (Bottom) Building blocks used for MOF preparation. The photochromic behavior of TNDS, BPMTC, and $BCMTC^{2-}$ as a function of UV and visible excitation is shown. The gray, red, dark blue, and light blue spheres represent C, O, N, and Cu atoms, respectively.

The metal choice for MOF preparation was determined by several factors: (i) the possibility to prepare a framework with photochromic linkers installed as pillars; (ii) tendency for reduction (comparable with the redox potentials of the chosen photochromic units in their excited states);[52−56] and (iii) the possibility to detect changes in oxidation states *in situ*. As a result, copper(II) salt was selected for photoresponsive MOF preparation. The copper-based frameworks have been synthesized through a transmetalation procedure,[57−59] and the d^9-paramagnetic nature of the copper(II) species allowed for probing changes in metal oxidation states *in situ* via EPR spectroscopy since Cu(II) ↔ Cu(I) switching would result in changes in the EPR signal.[60] Moreover, copper(II) species are relatively easy to reduce in comparison with, for instance, Co(II) or Ni(II) species.[61−64] As precursors, we synthesized the zinc-based MOFs: $Zn_{2.0}$(TNDS)(DBTD), $Zn_{2.0}$(BPMTC)-(DBTD), and $Zn_{2.0}$(DPB-CHO)(DBTD) (Figure 1; H_4DBTD = 3′,6′-dibromo-4′,5′-bis(4-carboxyphenyl)-[1,1′,2′,1″-terphenyl]-4,4″-dicarboxylic acid).[45,65] Material characterization of Zn-MOFs by PXRD and FTIR spectroscopy is provided in the Supporting Information (SI, Figures S2−S7). Framework transmetalation was carried out in a dimethylformamide

https://doi.org/10.1021/jacs.1c11984
J. Am. Chem. Soc. 2022, 144, 4457−4468

(DMF) solution of copper(II) nitrate over 7 days (see the SI for more details). After cation exchange, the resulting samples were extensively washed using a Soxhlet extraction procedure to remove residual copper species from the pores prior to MOF characterization. PXRD studies of the prepared frameworks demonstrated that transmetalated MOFs are isostructural to the zinc-based analogues (Figures S2–S4),[45,65] confirming preservation of framework integrity during the cation exchange process. The FTIR spectra can be found in Figures S5–S8. To estimate the degree of transmetalation, inductively coupled plasma mass spectrometry (ICP-MS) was employed. As a result, complete zinc-to-copper transmetalation was observed for $Cu_{2.0}$(BPMTC)(DBTD). In the case of $Cu_{1.9}Zn_{0.1}$(TNDS)(DBTD) and $Cu_{1.2}Zn_{0.8}$(DPB-CHO)-(DBTD), 95% and 60% of zinc cations were replaced by copper. Preparation of Cu(BCMTC)(MeOH) was carried out through direct synthesis by heating copper(II) chloride in the presence of H_2BCMTC in methanol at 60 °C for 30 min using water as a medium, followed by the addition of an aqueous solution of ethylenediamine (see the SI for more details).

A schematic representation of all prepared frameworks, $Cu_{2.0}$(BPMTC)(DBTD), $Cu_{1.9}Zn_{0.1}$(TNDS)(DBTD), and Cu(BCMTC)(MeOH), is shown in Figure 1. The single-crystal X-ray data are provided in Figures S10 ($Cu_{1.9}Zn_{0.1}$(TNDS)(DBTD)), S1 ($Cu_{1.2}Zn_{0.8}$(DPB-CHO)-(DBTD)), and S11 (Cu(BCMTC)(MeOH)). The $Cu_{2.0}$(BPMTC)(DBTD), $Cu_{1.9}Zn_{0.1}$(TNDS)(DBTD), and $Cu_{1.2}Zn_{0.8}$(DPB-CHO)(DBTD) structures are constructed from two-dimensional (2D) layers in which the tetradentate linkers, $DBTD^{4-}$, are connected by paddlewheel-based metal nodes in their equatorial positions (Figures 1, S1, S10, and S11). The $DBTD^{4-}$-based 2D layers are connected with the corresponding pillars, such as TNDS, BPMTC, or DPB-CHO, coordinated to the axial positions of the paddlewheel metal nodes. The selected framework topology (i.e., photochromic linkers integrated as pillars between 2D layers) is essential for promoting TNDS linker photoisomerization, which is accompanied by a large structural rearrangement (Figure 1).[31−33,45] The Cu(BCMTC)(MeOH) structure also consists of 2D layers; however, the layers contain photochromic $BCMTC^{2-}$ units bound to the equatorial positions of a copper paddlewheel, while axial metal node sites are occupied by coordinated methanol molecules (Figure S11). In other words, the Cu(BCMTC)(MeOH) framework is two-dimensional with no interlayer coordination. Notably, the proximity of the copper paddlewheel units in Cu(BCMTC)(MeOH) is closer (shortest inter-paddlewheel metal-to-metal (M−M) distance = 5.52 Å) than in $Cu_{1.9}Zn_{0.1}$(TNDS)(DBTD) (shortest inter-paddlewheel M−M distance = 11.5 Å).

Photophysical Studies. DR spectroscopic studies were used as a first step to evaluate the absorption profiles and photoisomerization rates of the prepared photoresponsive frameworks. In comparison with zinc-based MOFs, integration of copper cations complicated the DR spectra of the MOFs (Figures S12 and S13). For instance, in the spiropyran-based MOF, $Cu_{1.9}Zn_{0.1}$(TNDS)(DBTD), the appearance of an additional absorption band centered at 480 nm was detected (Figure S12). Notably, during the copper-to-zinc transmetalation procedure, copper cations not only can integrate inside the metal nodes but also can coordinate to the linker, as shown in Figure 2.[66] To investigate this effect further, we stored a mixture of (1′,3′-dihydro-1′,3′,3′-trimethyl-6-nitrospiro[2*H*-1-benzopyran-2,2′-(2*H*)-indole]; SP) and Cu-

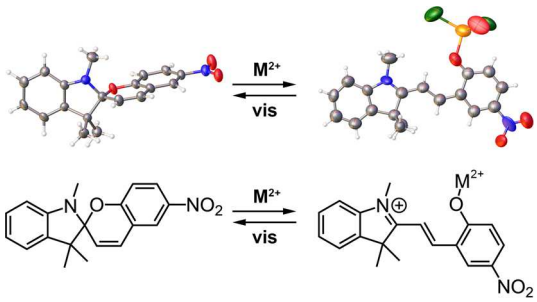

Figure 2. (Top) Single-crystal X-ray structure of spiropyran and merocyanine showing the reversible binding of M^{2+} (e.g., M = Cu or Zn).[66−69] Thermal displacement parameters are drawn at the 40% probability level. Gray, blue, orange, red, green, and white spheres represent C, N, Zn, O, Cl, and H atoms, respectively. (Bottom) Molecular representations of the crystal structures above.

$(NO_3)_2$ in tetrahydrofuran (THF) in the dark for 3 days after the measurements of the absorption profile were performed. As a result, a strong absorption band at 480 nm was detected (Figure S14), corresponding to chelation of Cu^{2+} to merocyanine, which is in line with the literature reports.[66−69] In addition, the intensity of this band changed upon altering the SP-to-$Cu(NO_3)_2$ ratio. We also found that the release of coordinated Cu(II) can be achieved through photoisomerization from the merocyanine to spiropyran isomer under 590 nm irradiation, resulting in the disappearance of the 480 nm band (Figure S14), which is in line with the literature reports demonstrating the release of M(II) cations upon visible irradiation (M = Cu and Zn; Figure 2).[66−71] We applied the aforementioned strategy of copper(II) release for treating the $Cu_{1.9}Zn_{0.1}$(TNDS)(DBTD) sample, before any spectroscopic measurements, to remove any complexity associated with the presence of copper cations chelated to the organic linker. We accomplished the release of copper(II) species through irradiation of the prepared MOF with 590 nm light, as indicated by the disappearance of the band at 480 nm (Figure S14). This treatment allowed us to deconvolute the effect of TNDS versus chelated copper cations monitored through the changes in the absorption profile.

The photochromic behavior of the synthesized frameworks was evaluated using DR spectroscopy through monitoring the attenuation of photoswitch isomerization (Figures 3, S15, and S16).[45] The MOF samples were exposed to UV irradiation (λ_{ex} = 365 nm) to convert the photochromic moieties into their respective colored forms, and the corresponding spectra of the photoswitch attenuation were collected over time (see more details in the SI). Diarylethene-based MOFs, ($Cu_{2.0}$(BPMTC)-(DBTD) and Cu(BCMTC)(MeOH), exhibited absorption bands centered at 540 and 580 nm, respectively, corresponding to the presence of photochromic units that attenuated over time with a reverse rate, $k_{reverse}$, of 3.2×10^{-3} and 2.0×10^{-2} s^{-1}, respectively (Figures 3 and S15). The determined $k_{reverse}$ for $Cu_{2.0}$(BPMTC)(DBTD) is similar to that of a previously reported diarylethene-based MOF (e.g., $Zn_{2.0}$(BPMTC)-(DBTD); 2.8×10^{-3} s^{-1}).[45] For the 2D layered structure, Cu(BCMTC)(MeOH), incomplete attenuation was observed over time; that is, the absorption profile did not change after 2 min of attenuation (Figure S15). Thus, the rate, $k_{reverse}$, for Cu(BCMTC)(MeOH) attenuation was determined from the first 30 s of attenuation.

https://doi.org/10.1021/jacs.1c11984
J. Am. Chem. Soc. 2022, 144, 4457−4468

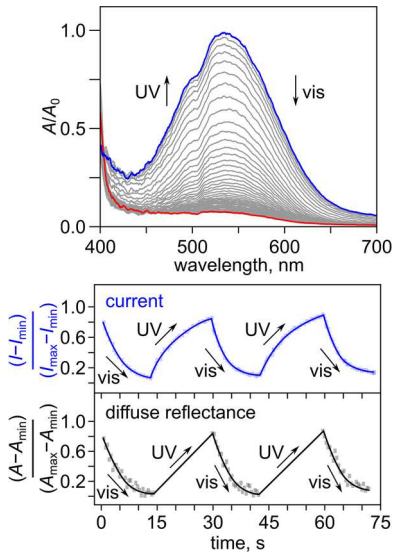

Figure 3. (Top) Normalized diffuse reflectance profile of diarylethene attenuation in $Cu_{2.0}$(BPMTC)(DBTD) after 30 s of UV (λ_{ex} = 365 nm) excitation and attenuation under visible light. (Bottom) Normalized current and optical cycling of photochromic $Cu_{2.0}$(BPMTC)(DBTD) through alternation of UV (λ_{ex} = 365 nm) and visible (λ_{ex} = 590 nm) irradiation. I_{max} and I_{min} = the maximum and minimum current values, respectively; A_{max} and A_{min} = the maximum and minimum absorbance values (converted from reflectance via the Kubelka−Munk function), respectively.

The estimated photoisomerization rate of BPMTC-integrated MOFs was slower in comparison with that observed for integrated TNDS moieties. In the case of $Cu_{1.9}Zn_{0.1}$(TNDS)-(DBTD), the rate, $k_{reverse}$, was determined to be 1.0×10^{-1} s^{-1}, which is similar to that of the Zn-based analogue (1.6×10^{-1} s^{-1}, Figure S16).[45] Such behavior can be explained by the fact that in the diarylethene-based MOFs the photoisomerization process affects the MOF skeleton since the photoswitch coordinates to metal nodes from both sides of the molecule,[45] while photoisomerization of the TNDS linker occurs within the pores.[45,65,72]

A photophysics−electronic property correlation was established through comparison of time-resolved DR and conductivity measurement data. We utilized a home-built *in situ* two-contact probe pressed-pellet setup[65,73,74] that allowed for monitoring the prepared MOFs' electronic response as a function of an excitation wavelength (more details in the SI). Initially, we monitored the changes in current, *I*, under a steady applied voltage, *V*, under alternating 15 s cycles of UV (λ_{ex} = 365 nm) and visible (λ_{ex} = 590 nm) irradiation. Current cycling for $Cu_{2.0}$(BPMTC)(DBTD) and $Cu_{1.9}Zn_{0.1}$(TNDS)-(DBTD) is shown in Figures 3 and S17, respectively. As a control experiment, we performed the same measurements for non-photochromic $Cu_{1.2}Zn_{0.8}$(DPB-CHO)(DBTD), and no significant changes in the current were detected upon exposure to either 365 or 590 nm irradiation (Figure S18). As shown in Figures 3 and S17, observed current cycling correlates with the changes in the MOFs' absorption profile (Figures S12 and S13). These observations are in line with the changes in density of states near the Fermi edge detected via XPS (Figure S19). Thus, the integration of photochromic moieties inside frameworks allowed us to dynamically control the electronic behavior of MOFs as a function of an excitation wavelength.

EPR Studies. Following electronic and optical measurements, we chose EPR spectroscopy to probe possible changes in the oxidation state of copper within the MOF metal nodes. If linker photoisomerization upon irradiation results, for instance, in reduction of copper from Cu(II) (d^9) to Cu(I) (d^{10}), it should be reflected through changes in the EPR signal.[60] Solid-state continuous-wave (CW) EPR spectroscopic studies were carried out on the MOF samples under UV (365 nm) and visible (590 nm) light.

For sample irradiation, two approaches were employed. In the first approach, the samples were irradiated *in situ*; that is, the photochromic MOFs were irradiated inside the EPR tubes using a mounted light-emitting diode (LED; λ_{ex} = 365 or 590 nm) and a fiber optic (see the SI for more details). As a control, prior to and between measurements, the fiber optic-loaded empty EPR tube was tested to ensure no chemical contaminations between the experiments. The *in situ* method of irradiation allowed us to study photochromic frameworks that possess rapid photoisomerization kinetics, such as $Cu_{1.9}Zn_{0.1}$(TNDS)(DBTD) ($k_{reverse}$ = 1.0×10^{-1} s^{-1}, as determined above). For photochromic samples with slower photoisomerization kinetics, such as $Cu_{2.0}$(BPMTC)(DBTD) (3.2×10^{-3} s^{-1}), *ex situ* sample irradiation can also be performed as an alternative approach (i.e., UV irradiation can occur outside of the EPR cavity) since the photoswitch attenuation (even in the presence of visible light) occurs during several hours.[45] To accomplish *ex situ* irradiation, the sample was carefully removed from the EPR cavity and exposed to 365 nm excitation wavelength (see the experimental details in the Supporting Information).

For $Cu_{2.0}$(BPMTC)(DBTD), containing the diarylethene-based photoswitch, we performed both *in situ* and *ex situ* irradiation experiments, while monitoring the X-band frequency (9.382 GHz) in the EPR spectrum and, therefore, the possible conversion of paramagnetic (Cu(II)) to diamagnetic (Cu(I)) centers. In the dark, an axial signal (i.e., $g_x = g_y \neq g_z$)) was observed at a *g*-value of 2.062 for $Cu_{2.0}$(BPMTC)(DBTD) (Figure 4) that could be assigned to monomeric Cu(II) or thermally populated antiferromagnetically coupled Cu(II).[75−79] The relative decrease in the EPR response was analyzed by double integration of the EPR spectra collected in the dark and under UV irradiation; then relative signal reduction (%) was estimated (see the SI for more details). Upon UV irradiation using the *in situ* approach for $Cu_{2.0}$(BPMTC)(DBTD), the Cu(II) signal (260−335 mT)[80−82] decreased by 11%, which we attributed to photoswitch-induced Cu(II) reduction (Figure S20).

To promote a more dramatic change in the EPR signal upon UV irradiation, we explored the *ex situ* irradiation method, as it would allow for a shorter LED-to-sample distance (i.e., higher photon flux) as well as access to a larger irradiation area (Figure S21). Indeed, the EPR signal of $Cu_{2.0}$(BPMTC)-(DBTD) was reduced by 32% upon only 30 min of *ex situ* UV exposure as opposed to 3 h for *in situ* irradiation leading to an 11% reduction (λ_{ex} = 365 nm for *ex situ* and *in situ* irradiation methods; Figures 4 and S20). For confirmation that the observed EPR signal attenuation was caused by Cu(II) reduction via photochromic units, we performed control experiments on an isostructural, non-photochromic, Cu-based MOF, $Cu_{1.2}Zn_{0.8}$(DPB-CHO)(DBTD). As clearly shown in Figure S22, there are no changes in the EPR profile of $Cu_{1.2}Zn_{0.8}$(DPB-CHO)(DBTD) upon UV irradiation using either *in situ* or *ex situ* irradiation methods (λ_{ex} = 365 nm).

https://doi.org/10.1021/jacs.1c11984
J. Am. Chem. Soc. 2022, 144, 4457−4468

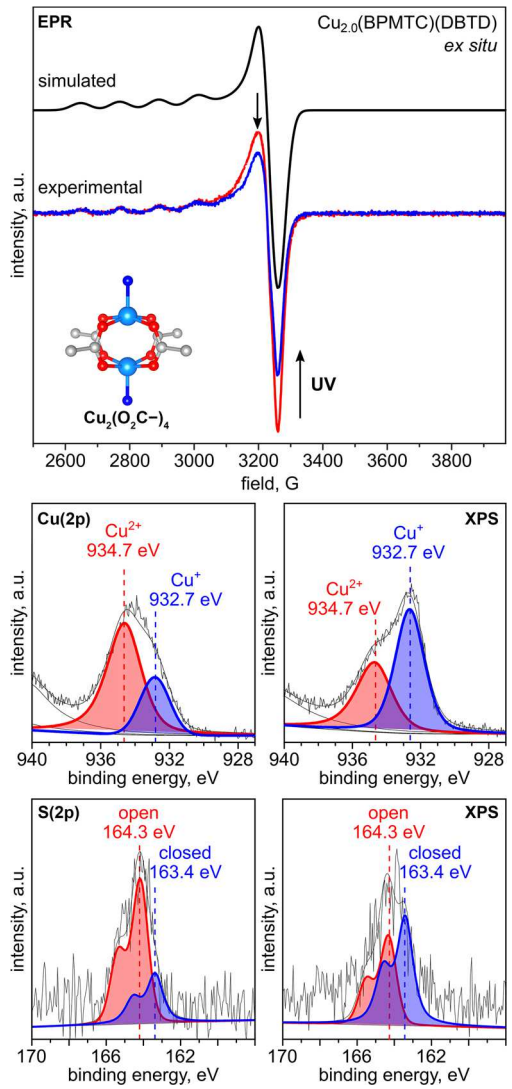

Figure 4. (Top) EPR spectra of $Cu_{2.0}$(BPMTC)(DBTD) before (red) and after (blue) 365 nm *ex situ* irradiation. The inset shows a paddlewheel metal node. The gray, red, dark blue, and light blue spheres represent C, O, N, and Cu atoms, respectively. The simulated spectrum is shown in black. (Middle) XPS data for the Cu(2p) region for $Cu_{2.0}$(BPMTC)(DBTD) in the dark (middle left) and under continuous UV irradiation (middle right). (Bottom) XPS data for the S(2p) region for $Cu_{2.0}$(BPMTC)(DBTD) in the dark (bottom left) and under continuous UV irradiation (bottom right).

Furthermore, two non-photochromic MOFs containing Cu(II) paddlewheel metal nodes, $Zn_{1.40}Cu_{1.60}(BTC)_2$ and $Zn_{1.95}Cu_{1.05}(BTC)_2$ (H_3BTC = 1,3,5-benzenetricarboxylic acid, Figures S23 and S24), were prepared and analyzed.[57,83] These samples also possessed similar hyperfine coupling resonances and a similar *g*-value (2.061) to that of $Cu_{2.0}$(BPMTC)(DBTD) (2.062). As expected, no changes in the intensity of the EPR signal were observed upon extensive UV exposure (Figure S25), confirming that the stimuli-responsive units were responsible for the observed changes in the Cu(II) signal reduction in photochromic MOFs. In addition, several Cu(II) and Cu(I) salts were analyzed under UV irradiation to further investigate the possible effect of UV excitation (Figures S26–S28). As expected, no changes in the EPR signal intensity were detected even after prolonged exposure to UV light using both *in situ* and *ex situ* methods (Figures S26–S28).

To correlate the sample area that underwent UV irradiation with the observed changes in the EPR signal, we compared the experimental and theoretical signal decrease based on irradiation area. For that, we constructed a simplified model to approximate the amount of sample influenced by UV light under our setup (Figure S21). In the *ex situ* approach, the sample was only irradiated from one side of the EPR tube to minimize sample disturbance upon removal from the EPR spectrometer cavity. The volume of the MOF sample in the irradiation area was estimated to be 14 mm^3 based on an approximation of UV light penetration depth (~0.8 mm) measured with vernier calipers (further details in the SI). The total sample in the tube was approximated as a cylinder of volume 35 mm^3, and thus, 40% of the sample was exposed to UV irradiation. As a result, the reduction of the EPR signal in the $Cu_{2.0}$(BPMTC)(DBTD) sample was found to be 32%, compared to the theoretical maximum of 40% estimated through irradiation area calculations (the *ex situ* approach; Figure S21). Using the *in situ* approach, the top (UV irradiated) and bottom (kept in the dark, Figure S21) portion of the cylinder were approximated using volumes of 5.6 and 29.4 mm^3, respectively. Therefore, 16% of the sample is in the irradiation area in the case of the *in situ* irradiation, which was in line with the observed changes in the Cu(II) EPR signal (11%; Figure S20).

To support our conclusions based on changes in the EPR spectra, we utilized XPS for *in situ* monitoring of changes in metal oxidation states.[84−87] Scanning the Cu(2p) region of $Cu_{2.0}$(BPMTC)(DBTD) in the dark, we observed a strong signal corresponding to Cu(II) and a small peak corresponding to Cu(I), which was determined previously to be due to a charging effect for Cu(II) paddlewheel-based MOFs (Figure 4).[86] After *in situ* UV irradiation for 18 h, we observed a significant decrease in the Cu(II) signal and enhancement of the Cu(I) signal. In fact, the change observed in the EPR spectrum (*ex situ* for $Cu_{2.0}$(BPMTC)(DBTD) = 32%) closely matched the observed changes detected in the XPS data (31%). Moreover, we also observed a 30% change in the intensity of the S(2p) electron binding energy (Figure 4), which corresponds to changes between the "closed" and "open" forms of the diarylethene linker (consistent with previous reports).[65] Therefore, both EPR and XPS studies demonstrated a correlation between the changes in the oxidation states and photoisomer conversion that coincide with optical property changes detected using DR spectroscopy. In the EPR spectrum collected for Cu(BCMTC)(MeOH), we observed a rhombic Cu(II)-centered signal (*g*-value = 2.061; Figure S29). Notably, the EPR signal from the Cu(BCMTC)-(MeOH) sample was much broader in comparison with $Cu_{2.0}$(BPMTC)(DBTD). Due to irreversible photochromic behavior (*vide infra*), we limited further studies performed for Cu(BCMTC)(MeOH). However, despite structural differences, we observed similar changes from the other two frameworks in the EPR spectrum upon UV irradiation, indicating that photochromic units can control the MOFs' paramagnetic behavior.

In the case of $Cu_{1.9}Zn_{0.1}$(TNDS)(DBTD), which rapidly photoisomerizes,[45] only the *in situ* irradiation method was suitable for performing EPR measurements (*vide supra*). It is important to note that prior to EPR experiments the $Cu_{1.9}Zn_{0.1}$(TNDS)(DBTD) sample was irradiated with 590

https://doi.org/10.1021/jacs.1c11984
J. Am. Chem. Soc. 2022, 144, 4457−4468

nm light, followed by extensive washing with DMF to remove any copper cations possibly coordinated to the merocyanine photoisomer, as discussed above. In the dark, prior to UV irradiation, the axial Cu(II) signal at a *g*-value of 2.061 (Figures 5 and S30) appeared nearly identical to that of

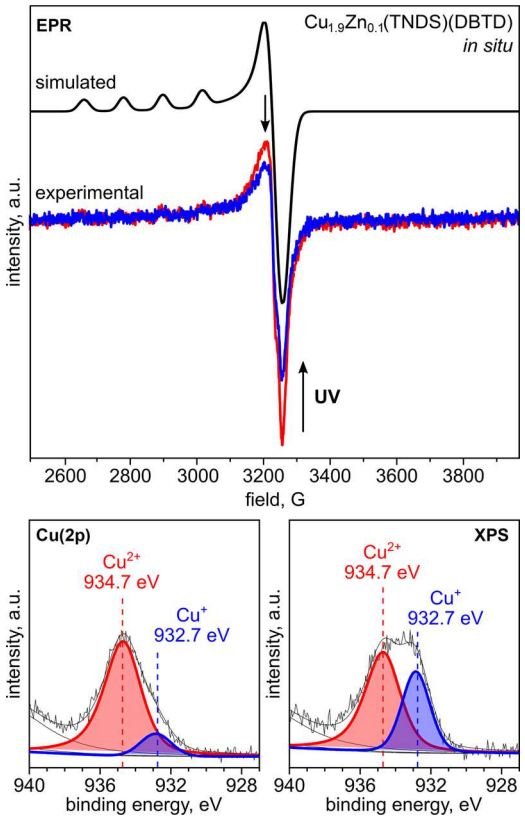

Figure 5. (Top) EPR spectra of $Cu_{1.9}Zn_{0.1}$(TNDS)(DBTD) before (red) and after (blue) 365 nm *ex situ* irradiation. The simulated spectrum is shown in black. XPS data for the Cu(2p) region for $Cu_{1.9}Zn_{0.1}$(TNDS)(DBTD) in the dark (bottom left) and under continuous UV irradiation (bottom right).

$Cu_{2.0}$(BPMTC)(DBTD) (Figure 4). Upon 30 min of *in situ* UV exposure, the signal was reduced by 8%, based on integrating the area under the curve of the EPR absorption spectrum. The observed changes in the copper oxidation state were also supported by XPS measurements. Scanning the Cu(2p) region before and after 18 h of UV exposure revealed a 24% increase in the Cu(I) signal (based on area by integration of the XPS spectrum), which was over three times larger than the *in situ* UV irradiation EPR experiments (8%; Figure 5). We attributed the observed difference in EPR and XPS results to a limited area of the sample that underwent irradiation during the EPR spectroscopic experiments (only the top section of the EPR tube) compared to UV exposure of the entire sampling area during XPS measurements (which is more similar to *ex situ* irradiation experiments). It is important to note that all detected changes in the EPR spectra were reversible. For instance, *in situ* irradiation of a fresh sample of $Cu_{1.9}Zn_{0.1}$(TNDS)(DBTD) with 365 nm light for 30 min reduced Cu(II) by 8%, while 590 nm irradiation for 30 min resulted in a 94% restoration of the EPR signal (Figure S31).

To study the correlation between the observed changes in the EPR spectra and reversibility of changes in metal oxidation states upon irradiation, we also probed chemical (irreversible) reduction of MOF copper centers. After the addition of 10 μL of a 1.0 M hydrazine THF solution to $Cu_{2.0}$(BPMTC)(DBTD), we monitored changes in the EPR signal at the X-band frequency. As expected, we observed a partial decrease of the EPR signal associated with Cu(II) reduction (Figure S32). Further addition of a more concentrated hydrazine solution to the MOF sample resulted in the formation of an EPR-silent sample, indicative of the complete reduction of Cu(II) metal centers. The PXRD pattern of the hydrazine-reduced sample also showed substantially diminished crystallinity (Figure S33).

To further shed light on the mechanism of Cu(II) reduction in the presence of MOF photochromic linkers, we employed cyclic voltammetry (CV) studies with the support of literature reports.[24,62,88−91] As a first step, we performed CV measurements on BPMTC and TNDS in the dark and under constant UV irradiation (λ_{ex} = 365 nm). For photochromic BPMTC (5.0 mM in acetonitrile (ACN), vs SCE, Figure S34), we observed no redox behavior in the dark; however, under UV irradiation, an irreversible oxidation wave at E_{ox} = 0.63 V was evident. An irreversible oxidation wave for TNDS (5.0 mM in ACN, vs SCE) was also observed (E_{ox} = 1.24 V) under UV irradiation (Figure S34). With this data in conjunction with the overlays of the absorption and emission spectra, we calculated the excited state potential using the following equation (eq 1):[63,64]

$$E_{ox}^{*} = E_{ox} - E_{0-0} \quad (1)$$

where E_{ox}* is the excited state oxidation potential, E_{ox} is the measured oxidation potential of the ground state, and E_{0-0} is the energy of the lowest energy excited state transition, estimated as the intercept of absorption and emission energy (Figure S35). Using this relationship, the calculated E_{ox}* values for TNDS and BPMTC are −0.80 and −1.29 V vs SCE, respectively. The literature value for the Cu(II/I) couple was observed at −0.31 V,[65] suggesting that the reduction of Cu(II) to Cu(I) is feasible through oxidation of BPMTC and TNDS excited states.[63,64]

There are several literature reports that support the formation of a radical cation of spiropyran- and diarylethene-based compounds upon photoirradiation,[52−56] and this process could potentially affect the observed photoinduced charge transfer. To further study this observation, we performed EPR measurements involving the addition of a radical trap, 5,5-dimethyl-1-pyrroline-N-oxide (DMPO), to the sample.[92−94] In the case of the diarylethene-based linker, an EPR spectrum of a THF solution of BPMTC (80 mM) and DMPO (40 mM) was first collected in the dark and after UV irradiation (more experimental details in the SI). As shown in Figure 6, we observed the appearance of a radical signal from the BPMTC−

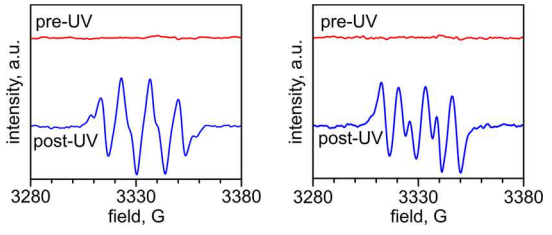

Figure 6. EPR spectra of an SP and DMPO solution in THF before (top left) and after (bottom left) UV irradiation (λ_{ex} = 365 nm). EPR spectra of a BPMTC and DMPO solution in THF before (top right) and after (bottom right) UV irradiation (λ_{ex} = 365 nm).

https://doi.org/10.1021/jacs.1c11984
J. Am. Chem. Soc. 2022, 144, 4457−4468

DMPO adduct with a *g*-value of 2.009 (Figure 6), which is in line with literature reports.[95,96] In the case of SP, we observed the appearance of a radical signal after UV irradiation of a THF solution of SP (80 mM) and DMPO (40 mM, Figure 6). The *g*-value was found to be 2.009 (Figure 6).[97−100] As a control experiment, a solution of DMPO in THF (in the absence of photochromic molecules) was irradiated with UV light, and no new EPR signal was observed (Figure S36).

To summarize, these results are consistent with the hypothesis that radical-mediated charge transfer (which was observed previously for diarylethene-containing molecular donor−acceptor pairs and complexes)[53,101] can promote the reduction of Cu(II) to Cu(I) in MOFs containing photochromic spiropyran- or diarylethene-based moieties.

Photoisomerization Quantum Yield Measurements. As a part of our studies performed on photochromic MOFs, it is important to probe photoisomerization quantum yield (φ_{PI}) of photochromic MOFs. The φ_{PI} value is a fundamental photophysical property that has been overlooked in photoresponsive MOFs,[32,34] despite being imperative for their practical implementation. In our case, we define φ_{PI} for the first time for the forward photoisomerization process (i.e., upon irradiation with UV light).[102−105]

In the case of diarylethene derivatives integrated inside a rigid MOF matrix, φ_{PI} could be greatly enhanced by aligning the chromophores in an antiparallel confirmation (as opposed to parallel; Figure 7).[106−110] In solution, parallel and antiparallel conformers of diarylethene and its derivatives are typically present in nearly equal proportions.[111,112] However, confinement-restricted diarylethene compounds could exhibit high φ_{PI} due to elimination of the parallel confirmation, as previously shown on the example of cyclodextrin cavities[113,114] or organic crystalline lattices.[106,115,116] In contrast, spiropyran and its derivatives undergo a rapid internal conversion (from the S_1 to S_2 states of spiropyran),[117,118] limiting φ_{PI} to 10% for spiropyran derivatives. Thus, we anticipate a much more pronounced effect on diarylethene-integrated linkers compared to spiropyran-based ones.

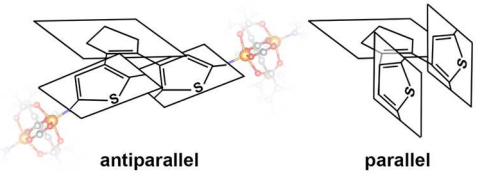

compound	$k_{forward}$, ms^{-1}	*T*, %	φ_{PI}, %
$Cu_{1.9}Zn_{0.1}$(TNDS)(DBTD)	3.6	27 ± 0.3	8 ± 0.9
$Cu_{2.0}$(BPMTC)(DBTD)	9.7	14 ± 1.3	79 ± 1.5
Aberchrome 670	6.2	96 ± 0.5	27[a]

[a] value obtained from *Sci. Rep.*, **2017**, *7*, 41145.

Figure 7. Schematic representation of the (top left) antiparallel and (top right) parallel confirmations of diarylethene. In the case of the antiparallel conformation, coordination to the MOF metal node is outlined. (Bottom) Forward photoisomerization rates ($k_{forward}$), transmission (*T*, %) at λ_{ex} = 365 nm, and photoisomerization quantum yields (φ_{PI}) for diarylethene- and spiropyran-containing MOFs.

For the determination of φ_{PI}, we first prepared Aberchrome 670 films of known thickness and φ_{PI} of 27% using an established literature procedure.[102] The photoisomerization quantum yield was determined using the following relationship (eq 2):[102]

$$\frac{\varphi_{A670}\varepsilon_{A670}(1 - T_{A670})}{k_{forward(A_{670})}} = \frac{\varphi_{crystal}\varepsilon_{crystal}(1 - T_{crystal})}{k_{forward(crystal)}} \quad (2)$$

where *T* is the transmission at an excitation wavelength (λ_{ex} = 365 nm), ε is the molar extinction coefficient of the chromophore at the monitoring wavelength (e.g., $\lambda_{(abs)max}$ = 601 nm for TNDS), and $k_{forward}$ is the rate of the forward process.[102] The increase in absorption (decrease in transmission) was recorded over time and fit with a first-order rate equation to estimate the forward reaction rate.[31,35,119−123] More experimental details and the procedure implemented can be found in the SI. A summary of the acquired results is illustrated in Figure 7. Thus, φ_{PI} for $Cu_{2.0}$(BPMTC)(DBTD) was found to be as high as 79% in the MOF, compared to, for instance, 21−40% observed for molecular arrays of diarylethene oligomers[115] and 21−50% detected for diarylethene derivatives in solution (3,3′-(perfluorocyclopent-1-ene-1,2-diyl)bis(2,4-dimethylthiophene) and 3,3′-(perfluorocyclopent-1-ene-1,2-diyl)bis(2-methyl-5-phenylthiophene)).[115,116] In fact, φ_{PI} for diarylethene derivatives in solution cannot exceed 50% due to a nearly equal ratio of parallel and antiparallel conformations.[116]

As expected, a MOF matrix imposes conformational restriction on the BPMTC linker through elimination of the parallel confirmation, and therefore, enhancement of φ_{PI} was detected. In contrast to the diarylethene-based MOF, we found φ_{PI} of TNDS photoisomerization to be 8% in $Cu_{1.9}Zn_{0.1}$(TNDS)(DBTD), demonstrating a solution-like behavior. Specifically, the value of φ_{PI} for $Cu_{1.9}Zn_{0.1}$(TNDS)-(DBTD) is similar to that reported for spiropyran in solutions (e.g., 5−9%),[124−126] likely due to rapid internal conversion and large geometric reorganization.[117,118] The experimentally observed 79% and 8% values of φ_{PI} are the first reports in the area of photochromic MOFs demonstrating the advantages of a framework rigid matrix: (i) selective elimination of the parallel confirmation and φ_{PI} enhancement for coordinatively immobilized diarylethene derivatives and (ii) possibility to overcome challenges associated with limited photoisomerization of spiropyran derivatives in the solid state.[31,35,45]

CONCLUSION

We report a novel concept of reversible modulation of metal oxidation states in metal−organic frameworks through integration of photochromic moieties as a function of an excitation wavelength. On the example of three novel copper-based diarylethene- and spiropyran-containing frameworks, we observed switching between Cu(II) and Cu(I) states upon UV and visible light alternation. We monitored the changes in material properties through a combination of powder and single-crystal X-ray diffraction, conductivity measurements, cyclic voltammetry, and electron paramagnetic resonance, X-ray photoelectron, and diffuse reflectance spectroscopies. Photochromic behavior and the corresponding changes in the frameworks' electronic properties were also demonstrated, including determination of the forward and reverse rates for the photoisomerization processes. Finally, photoisomerization quantum yields of photochromic moieties coordinatively immobilized within a porous matrix were determined for the first time. To summarize, the surface of tuning photoswitchable molecules' oxidation states has only been scratched, and we

https://doi.org/10.1021/jacs.1c11984
J. Am. Chem. Soc. 2022, 144, 4457−4468

believe that a thrust of research in this direction is imminent and will greatly impact the expanding materials landscape.

■ ASSOCIATED CONTENT

Supporting Information

The Supporting Information is available free of charge at https://pubs.acs.org/doi/10.1021/jacs.1c11984.

Additional experimental details, X-ray structure refinement data, ICP-MS data, PXRD patterns, cyclic voltammograms, DR, FTIR, XPS, UV−vis, and EPR spectra (PDF)

Accession Codes

CCDC 2121194−2121196 contain the supplementary crystallographic data for this paper. These data can be obtained free of charge via www.ccdc.cam.ac.uk/data_request/cif, or by emailing data_request@ccdc.cam.ac.uk, or by contacting The Cambridge Crystallographic Data Centre, 12 Union Road, Cambridge CB2 1EZ, UK; fax: +44 1223 336033.

■ AUTHOR INFORMATION

Corresponding Author

Natalia B. Shustova − *Department of Chemistry and Biochemistry, University of South Carolina, Columbia, South Carolina 29208, United States;* orcid.org/0000-0003-3952-1949; Email: shustova@sc.edu

Authors

Corey R. Martin − *Department of Chemistry and Biochemistry, University of South Carolina, Columbia, South Carolina 29208, United States*

Kyoung Chul Park − *Department of Chemistry and Biochemistry, University of South Carolina, Columbia, South Carolina 29208, United States*

Gabrielle A. Leith − *Department of Chemistry and Biochemistry, University of South Carolina, Columbia, South Carolina 29208, United States*

Jierui Yu − *Department of Chemistry and Biochemistry, University of South Carolina, Columbia, South Carolina 29208, United States;* orcid.org/0000-0001-8422-3583

Abhijai Mathur − *Department of Chemistry and Biochemistry, University of South Carolina, Columbia, South Carolina 29208, United States*

Gina R. Wilson − *Department of Chemistry and Biochemistry, University of South Carolina, Columbia, South Carolina 29208, United States*

Gayathri B. Gange − *Department of Chemistry and Biochemistry, University of South Carolina, Columbia, South Carolina 29208, United States*

Emily L. Barth − *Department of Chemistry, Yale University, New Haven, Connecticut 06520, United States*

Richard T. Ly − *Department of Chemistry and Biochemistry, University of South Carolina, Columbia, South Carolina 29208, United States*

Olivia M. Manley − *Department of Chemistry, North Carolina State University, Raleigh, North Carolina 27695, United States*

Kelly L. Forrester − *Department of Chemistry and Biochemistry, University of South Carolina, Columbia, South Carolina 29208, United States*

Stavros G. Karakalos − *College of Engineering and Computing, University of South Carolina, Columbia, South Carolina 29208, United States;* orcid.org/0000-0002-3428-5433

Mark D. Smith − *Department of Chemistry and Biochemistry, University of South Carolina, Columbia, South Carolina 29208, United States*

Thomas M. Makris − *Department of Chemistry, North Carolina State University, Raleigh, North Carolina 27695, United States;* orcid.org/0000-0001-7927-620X

Aaron K. Vannucci − *Department of Chemistry and Biochemistry, University of South Carolina, Columbia, South Carolina 29208, United States;* orcid.org/0000-0003-0401-7208

Dmitry V. Peryshkov − *Department of Chemistry and Biochemistry, University of South Carolina, Columbia, South Carolina 29208, United States;* orcid.org/0000-0002-5653-9502

Complete contact information is available at: https://pubs.acs.org/10.1021/jacs.1c11984

Author Contributions

The manuscript was written through contributions of all authors. All authors have given approval to the final version of the manuscript.

Notes

The authors declare no competing financial interest.

■ ACKNOWLEDGMENTS

The authors are grateful for support from the NSF CAREER Award (DMR-1553634), NSF Award (DMR-2103722), SC EPSCoR GEAR, and a Cottrell Scholar Award from the Research Corporation for Science Advancement. N.B.S. also acknowledges support from the Dreyfus Teaching-Scholar Award supported by the Dreyfus Foundation and the Hans Fischer Fellowship.

■ REFERENCES

(1) Chen, Y.; Zhang, X.; Wang, X.; Drout, R. J.; Mian, M. R.; Cao, R.; Ma, K.; Xia, Q.; Li, Z.; Farha, O. K. Insights into the Structure-Activity Relationship in Aerobic Alcohol Oxidation over a Metal-Organic-Framework-Supported Molybdenum(VI) Catalyst. *J. Am. Chem. Soc.* **2021**, *143*, 4302−4310.

(2) Fang, Y.; Powell, J. A.; Li, E.; Wang, Q.; Perry, Z.; Kirchon, A.; Yang, X.; Xiao, Z.; Zhu, C.; Zhang, L.; Huang, F.; Zhou, H.-C. Catalytic Reactions within the Cavity of Coordination Cages. *Chem. Soc. Rev.* **2019**, *48*, 4707−4730.

(3) Zhao, S. Y.; Zhang, B.; Su, H.; Zhang, J. J.; Li, X. H.; Wang, K. X.; Chen, J. S.; Wei, X.; Feng, P. Enhanced Oxygen Electroreduction over Nitrogen-Free Carbon Nanotube-Supported $CuFeO_2$ Nanoparticles. *J. Mater. Chem. A* **2018**, *6*, 4331−4336.

(4) Karges, J.; Stokes, R. W.; Cohen, S. M. Metal Complexes for Therapeutic Applications. *Trends Chem.* **2021**, *3*, 523−534.

(5) Liu, W.; Fang, Y.; Li, J. Copper Iodide Based Hybrid Phosphors for Energy-Efficient General Lighting Technologies. *Adv. Funct. Mater.* **2018**, *28*, 1705593.

(6) Li, S.; Gao, Y.; Li, N.; Ge, L.; Bu, X.; Feng, P. Transition Metal-Based Bimetallic MOFs and MOF-Derived Catalysts for Electrochemical Oxygen Evolution Reaction. *Energy Environ. Sci.* **2021**, *14*, 1897−1927.

(7) Gerkman, M. A.; Gibson, R. S. L.; Calbo, J.; Shi, Y.; Fuchter, M. J.; Han, G. G. D. Arylazopyrazoles for Long-Term Thermal Energy Storage and Optically Triggered Heat Release below 0 °C. *J. Am. Chem. Soc.* **2020**, *142*, 8688−8695.

(8) Zhou, W.; Huang, D.; Wu, Y.; Zhao, J.; Wu, T.; Zhang, J.; Li, D.; Sun, C.; Feng, P.; Bu, X. Stable Hierarchical Bimetal−Organic

Nanostructures as Highperformance Electrocatalysts for the Oxygen Evolution Reaction. *Angew. Chem., Int. Ed.* **2019**, *58*, 4227−4231.
(9) Yang, Y.; Zhang, X.; Kanchanakungwankul, S.; Lu, Z.; Noh, H.; Syed, Z. H.; Farha, O. K.; Truhlar, D. G.; Hupp, J. T. Unexpected "Spontaneous" Evolution of Catalytic, MOF-Supported Single Cu(II) Cations to Catalytic, MOF-Supported Cu(0) Nanoparticles. *J. Am. Chem. Soc.* **2020**, *142*, 21169−21177.
(10) Cadiau, A.; Kolobov, N.; Srinivasan, S.; Goesten, M. G.; Haspel, H.; Bavykina, A. V.; Tchalala, M. R.; Maity, P.; Goryachev, A.; Poryvaev, A. S.; Eddaoudi, M.; Fedin, M. V.; Mohammed, O. F.; Gascon, J. A Titanium Metal-Organic Framework with Visible-Light-Responsive Photocatalytic Activity. *Angew. Chem., Int. Ed.* **2020**, *59*, 13468−13472.
(11) Park, J.; Jiang, Q.; Feng, D.; Zhou, H.-C. Controlled Generation of Singlet Oxygen in Living Cells with Tunable Ratios of the Photochromic Switch in Metal-Organic Frameworks. *Angew. Chem., Int. Ed.* **2016**, *55*, 7188−7193.
(12) Liu, X.; Kirlikovali, K. O.; Chen, Z.; Ma, K.; Idrees, K. B.; Cao, R.; Zhang, X.; Islamoglu, T.; Liu, Y.; Farha, O. K. Small Molecules, Big Effects: Tuning Adsorption and Catalytic Properties of Metal-Organic Frameworks. *Chem. Mater.* **2021**, *33*, 1444−1454.
(13) Wang, X. N.; Zhao, Y.; Li, J. L.; Pang, J. D.; Wang, Q.; Li, B.; Zhou, H.-C. Biomimetic Catalysts of Iron-Based Metal-Organic Frameworks with High Peroxidase-Mimicking Activity for Colorimetric Biosensing. *Dalton Trans.* **2021**, *50*, 3854−3861.
(14) Kalaj, M.; Cohen, S. M. Postsynthetic Modification: An Enabling Technology for the Advancement of Metal-Organic Frameworks. *ACS Cent. Sci.* **2020**, *6*, 1046−1057.
(15) Yang, S.; Hu, W.; Nyakuchena, J.; Fiankor, C.; Liu, C.; Kinigstein, E. D.; Zhang, J.; Zhang, X.; Huang, J. Unravelling a Long-Lived Ligand-to-Metal Cluster Charge Transfer State in Ce−TCPP Metal Organic Frameworks. *Chem. Commun.* **2020**, *56*, 13971−13974.
(16) Murase, R.; Leong, C. F.; D'Alessandro, D. M. Mixed Valency as a Strategy for Achieving Charge Delocalization in Semiconducting and Conducting Framework Materials. *Inorg. Chem.* **2017**, *56*, 14373−14382.
(17) Park, J. G.; Aubrey, M. L.; Oktawiec, J.; Chakarawet, K.; Darago, L. E.; Grandjean, F.; Long, G. J.; Long, J. R. Charge Delocalization and Bulk Electronic Conductivity in the Mixed-Valence Metal-Organic Framework $Fe(1,2,3\text{-Triazolate})_2(BF_4)_X$. *J. Am. Chem. Soc.* **2018**, *140*, 8526−8534.
(18) Xie, L. S.; Sun, L.; Wan, R.; Park, S. S.; DeGayner, J. A.; Hendon, C. H.; Dincă, M. Tunable Mixed-Valence Doping toward Record Electrical Conductivity in a Three-Dimensional Metal-Organic Framework. *J. Am. Chem. Soc.* **2018**, *140*, 7411−7414.
(19) Hei, X.; Teat, S. J.; Liu, W.; Li, J. Eco-Friendly, Solution-Processable and Efficient Low-Energy Lighting Phosphors: Copper Halide Based Hybrid Semiconductors $Cu_4X_6(L)_2$ (X = Br, I) Composed of Covalent, Ionic and Coordinate Bonds. *J. Mater. Chem. C* **2020**, *8*, 16790−16797.
(20) Sabury, S.; Adams, T. J.; Kocherga, M.; Kilbey, S. M.; Walter, M. G. Synthesis and Optoelectronic Properties of Benzodithiophene-Based Conjugated Polymers with Hydrogen Bonding Nucleobase Side Chain Functionality. *Polym. Chem.* **2020**, *11*, 5735−5749.
(21) Zhou, Z.; Mukherjee, S.; Hou, S.; Li, W.; Elsner, M.; Fischer, R. A. Porphyrinic MOF Film for Multifaceted Electrochemical Sensing. *Angew. Chem., Int. Ed.* **2021**, *60*, 20551−20557.
(22) Noh, H.; Jeon, N.; Martinson, A. B. F.; Hupp, J. T. Stabilization of Low Valent Zirconium Nitrides in Titanium Nitride via Plasma-Enhanced Atomic Layer Deposition and Assessment of Electrochemical Properties. *ACS Appl. Energy Mater.* **2020**, *3*, 5095−5100.
(23) Owens-Baird, B.; Wang, J.; Wang, S. G.; Chen, Y. S.; Lee, S.; Donadio, D.; Kovnir, K. III-V Clathrate Semiconductors with Outstanding Hole Mobility: $Cs_8In_{27}Sb_{19}$ and $A_8Ga_{27}Sb_{19}$ (A = Cs, Rb). *J. Am. Chem. Soc.* **2020**, *142*, 2031−2041.
(24) Batool, S. S.; Gilani, S. R.; Tahir, M. N.; Siddique, A.; Harrison, W. T. A. Crystal Structure and Spectroscopic Characterization of a Coordination Polymer of Copper(II) Chloride with Ethylenediamine and the 2-Hydroxybenzoate Ion. *J. Struct. Chem.* **2016**, *57*, 1176−1181.
(25) Gonçalves, B. F.; LaGrow, A. P.; Pyrlin, S.; Owens-Baird, B.; Botelho, G.; Marques, L. S. A.; Ramos, M. M. D.; Kovnir, K.; Lanceros-Mendez, S.; Kolen'ko, Y. V. Large-Scale Synthesis of Semiconducting $Cu(In,Ga)Se_2$ Nanoparticles for Screen Printing Application. *Nanomaterials* **2021**, *11*, 1148.
(26) Li, C.; Wang, K.; Li, J.; Zhang, Q. Recent Progress in Stimuli-Responsive Two-Dimensional Metal-Organic Frameworks. *ACS Materials Lett.* **2020**, *2*, 779−797.
(27) Zhang, H.; Cheng, H.-M.; Ye, P. 2D nanomaterials: beyond graphene and transition metal dichalcogenides. *Chem. Soc. Rev.* **2018**, *47*, 6009−6012.
(28) de Ruiter, G.; Tartakovsky, E.; Oded, N.; van der Boom, M. E. Sequential Logic Operations with Surface-Confined Polypyridyl Complexes Displaying Molecular Random Access Memory Features. *Angew. Chem., Int. Ed.* **2010**, *49*, 169−172.
(29) Pal, S.; Sen, B.; Lohar, S.; Mukherjee, M.; Banerjee, S.; Chattopadhyay, P. Effect of Metal Oxidation State on FRET: A Cu(I) Silent but Selectively Cu(II) Responsive Fluorescent Reporter and Its Bioimaging Applications. *Dalton Trans.* **2015**, *44*, 1761−1768.
(30) Blunden, B. M.; Stenzel, M. H. Incorporating Ruthenium into Advanced Drug Delivery Carriers − an Innovative Generation of Chemotherapeutics. *J. Chem. Technol. Biotechnol.* **2015**, *90*, 1177−1195.
(31) Klajn, R. Spiropyran-Based Dynamic Materials. *Chem. Soc. Rev.* **2014**, *43*, 148−184.
(32) Rice, A. M.; Martin, C. R.; Galitskiy, V. A.; Berseneva, A. A.; Leith, G. A.; Shustova, N. B. Photophysics Modulation in Photoswitchable Metal-Organic Frameworks. *Chem. Rev.* **2020**, *120*, 8790−8813.
(33) Leith, G. A.; Martin, C. R.; Mathur, A.; Kittikhunnatham, P.; Park, K. C.; Shustova, N. B. Dynamically Controlled Electronic Behavior of Stimuli-Responsive Materials: Exploring Dimensionality and Connectivity. *Adv. Energy Mater.* **2022**, *12*, 2100441.
(34) Castellanos, S.; Kapteijn, F.; Gascon, J. Photoswitchable Metal Organic Frameworks: Turn on the Lights and Close the Windows. *CrystEngComm* **2016**, *18*, 4006−4012.
(35) Morimoto, M.; Irie, M. Photochromism of Diarylethene Single Crystals: Crystal Structures and Photochromic Performance. *Chem. Commun.* **2005**, 3895−3905.
(36) Dolgopolova, E. A.; Rice, A. M.; Martin, C. R.; Shustova, N. B. Photochemistry and Photophysics of MOFs: Steps towards MOF-Based Sensing Enhancements. *Chem. Soc. Rev.* **2018**, *47*, 4710−4728.
(37) Chi, Z.; Zhang, X.; Xu, B.; Zhou, X.; Ma, C.; Zhang, Y.; Liu, S.; Xu, J. Recent Advances in Organic Mechanofluorochromic Materials. *Chem. Soc. Rev.* **2012**, *41*, 3878−3896.
(38) Andrzejewski, M.; Katrusiak, A. Piezochromic Porous Metal-Organic Framework. *J. Phys. Chem. Lett.* **2017**, *8*, 279−284.
(39) Zhang, Y.; Hu, W.; Wang, D.; Reinhart, B. J.; Huang, J. Electron Shuttle in the MOF Derived TiO_2/CuO Heterojunction Boosts Light Driven Hydrogen Evolution. *J. Mater. Chem. A* **2021**, *9*, 6180−6187.
(40) Small, L. J.; Schindelholz, M. E.; Nenoff, T. M. Hold on Tight: MOF-Based Irreversible Gas Sensors. *Ind. Eng. Chem. Res.* **2021**, *60*, 7998−8006.
(41) Fan, Z.; Wang, Z.; Cokoja, M.; Fischer, R. A. Defect Engineering: An Effective Tool for Enhancing the Catalytic Performance of Copper-MOFs for the Click Reaction and the A^3 Coupling. *Catal. Sci. Technol.* **2021**, *11*, 2396−2402.
(42) He, Y.; Yang, S.; Fu, Y.; Wang, F.; Ma, J.; Wang, G.; Chen, G.; Wang, M.; Dong, R.; Zhang, P.; Feng, X. Electronic Doping of Metal-Organic Frameworks for High-Performance Flexible Micro-Supercapacitors. *Small Struct.* **2021**, *2*, 2000095.
(43) Liu, J. J.; Guan, Y. F.; Li, L.; Chen, Y.; Dai, W. X.; Huang, C. C.; Lin, M. J. Construction of a Bicontinuous Donor−Acceptor Hybrid Material at the Molecular Level by Inserting Inorganic Nanowires into Porous MOFs. *Chem. Commun.* **2017**, *53*, 4481−4484.

https://doi.org/10.1021/jacs.1c11984
J. Am. Chem. Soc. 2022, 144, 4457−4468

(44) Jhang, P. C.; Chuang, N. T.; Wang, S. L. Layered Zinc Phosphates with Photoluminescence and Photochromism: Chemistry in Deep Eutectic Solvents. *Angew. Chem., Int. Ed.* **2010**, *49*, 4200−4204.
(45) Williams, D. E.; Martin, C. R.; Dolgopolova, E. A.; Swifton, A.; Godfrey, D. C.; Ejegbavwo, O. A.; Pellechia, P. J.; Smith, M. D.; Shustova, N. B. Flipping the Switch: Fast Photoisomerization in a Confined Environment. *J. Am. Chem. Soc.* **2018**, *140*, 7611−7622.
(46) Irie, M.; Lifka, T.; Uchida, K.; Kobatake, S.; Shindo, Y. Fatigue Resistant Properties of Photochromic Dithienylethenes: By-Product Formation. *Chem. Commun.* **1999**, 747−750.
(47) Tani, K.; Ishibashi, Y.; Miyasaka, H.; Kobatake, S.; Irie, M. Dynamics of Cyclization, Cycloreversion, and Multiphoton-Gated Reaction of a Photochromic Diarylethene Derivative in Crystalline Phase. *J. Phys. Chem. C* **2008**, *112*, 11150−11157.
(48) Irie, M.; Fukaminato, T.; Matsuda, K.; Kobatake, S. Photochromism of Diarylethene Molecules and Crystals: Memories, Switches, and Actuators. *Chem. Rev.* **2014**, *114*, 12174−12277.
(49) Tam, E. S.; Parks, J. J.; Shum, W. W.; Zhong, Y. W.; Santiago-Berríos, M. B.; Zheng, X.; Yang, W.; Chan, G. K. L.; Abruña, H. D.; Ralph, D. C. Single-Molecule Conductance of Pyridine-Terminated Dithienylethene Switch Molecules. *ACS Nano* **2011**, *5*, 5115−5123.
(50) Williams, D. E.; Rietman, J. A.; Maier, J. M.; Tan, R.; Greytak, A. B.; Smith, M. D.; Krause, J. A.; Shustova, N. B. Energy Transfer on Demand: Photoswitch-Directed Behavior of Metal-Porphyrin Frameworks. *J. Am. Chem. Soc.* **2014**, *136*, 11886−11889.
(51) Dolgopolova, E. A.; Williams, D. E.; Greytak, A. B.; Rice, A. M.; Smith, M. D.; Krause, J. A.; Shustova, N. B. A Bio-Inspired Approach for Chromophore Communication: Ligand-to-Ligand and Host-to-Guest Energy Transfer in Hybrid Crystalline Scaffolds. *Angew. Chem., Int. Ed.* **2015**, *54*, 13639−13643.
(52) Steen, J. D.; Duijnstee, D. R.; Sardjan, A. S.; Martinelli, J.; Kortekaas, L.; Jacquemin, D.; Browne, W. R. Electrochemical Ring-Opening and -Closing of a Spiropyran. *J. Phys. Chem. A* **2021**, *125*, 3355−3361.
(53) Morimoto, M.; Kobatake, S.; Irie, M. Photochromism of a Diarylethene Charge-Transfer Complex: Photochemical Control of Intermolecular Charge-Transfer Interaction. *Chem. Commun.* **2006**, 2656−2658.
(54) Healey, K.; Liang, W.; Southon, P. D.; Church, T. L.; D'Alessandro, D. M. Photoresponsive Spiropyran-Functionalised MOF-808: Postsynthetic Incorporation and Light Dependent Gas Adsorption Properties. *J. Mater. Chem. A* **2016**, *4*, 10816−10819.
(55) Moriyama, Y.; Matsuda, K.; Tanifuji, N.; Irie, S.; Irie, M. Electrochemical Cyclization/Cycloreversion Reactions of Diarylethenes. *Org. Lett.* **2005**, *7*, 3315−3318.
(56) Hakouk, K.; Oms, O.; Dolbecq, A.; Marrot, J.; Saad, A.; Mialane, P.; El Bekkachi, H.; Jobic, S.; Deniard, P.; Dessapt, R. New Photoresponsive Charge-Transfer Spiropyran/Polyoxometalate Assemblies with Highly Tunable Optical Properties. *J. Mater. Chem. C* **2014**, *2*, 1628−1641.
(57) Ejegbavwo, O. A.; Berseneva, A. A.; Martin, C. R.; Leith, G. A.; Pandey, S.; Brandt, A. J.; Park, K. C.; Mathur, A.; Farzandh, S.; Klepov, V. V.; Heiser, B. J.; Chandrashekhar, M.; Karakalos, S. G.; Smith, M. D.; Phillpot, S. R.; Garashchuk, S.; Chen, D. A.; Shustova, N. B. Heterometallic Multinuclear Nodes Directing MOF Electronic Behavior. *Chem. Sci.* **2020**, *11*, 7379−7389.
(58) Metavarayuth, K.; Ejegbavwo, O.; McCarver, G.; Myrick, M. L.; Makris, T. M.; Vogiatzis, K. D.; Senanayake, S. D.; Manley, O. M.; Ebrahim, A. M.; Frenkel, A. I.; Hwang, S.; Rajeshkumar, T.; Jimenez, J. D.; Chen, K.; Shustova, N. B.; Chen, D. A. Direct Identification of Mixed-Metal Centers in Metal-Organic Frameworks: $Cu_3(BTC)_2$ Transmetalated with Rh^{2+} Ions. *J. Phys. Chem. Lett.* **2020**, *11*, 8138−8144.
(59) Zhang, S.; Cheng, P. Recent Advances in the Construction of Lanthanide-Copper Heterometallic Metal-Organic Frameworks. *CrystEngComm* **2015**, *17*, 4250−4271.
(60) Godiksen, A.; Stappen, F. N.; Vennestrøm, P. N. R.; Giordanino, F.; Rasmussen, S. B.; Lundegaard, L. F.; Mossin, S. Coordination Environment of Copper Sites in Cu-CHA Zeolite Investigated by Electron Paramagnetic Resonance. *J. Phys. Chem. C* **2014**, *118*, 23126−23138.
(61) Hush, N. S.; Woolsey, I. S. A Study of the Reduced Species of Cobalt and Nickel Complexes Analogous to Vitamin B_{12}. *J. Am. Chem. Soc.* **1972**, *94*, 4107−4114.
(62) Xiao, Z.; Natarajan, M.; Zhong, W.; Liu, X. Probing into the Electrochemistry of Four Nickel(II) and Cobalt(II) Complexes with Azadiphosphine Ligands (PNP) and Their Catalysis on Proton Reduction. *Electrochim. Acta* **2020**, *340*, 135998.
(63) Comba, P.; Löhr, A. M.; Pfaff, F.; Ray, K. Redox Potentials of High-Valent Iron-, Cobalt-, and Nickel-Oxido Complexes: Evidence for Exchange Enhanced Reactivity. *Isr. J. Chem.* **2020**, *60*, 957−962.
(64) Ershova, I. V.; Smolyaninov, I. V.; Bogomyakov, A. S.; Fedin, M. V.; Starikov, A. G.; Cherkasov, A. V.; Fukin, G. K.; Piskunov, A. V. Tetrahedral Nickel(II) and Cobalt(II) Bis-*o*-Iminobenzosemiquinonates. *Dalton Trans.* **2019**, *48*, 10723−10732.
(65) Dolgopolova, E. A.; Galitskiy, V. A.; Martin, C. R.; Gregory, H. N.; Yarbrough, B. J.; Rice, A. M.; Berseneva, A. A.; Ejegbavwo, O. A.; Stephenson, K. S.; Kittikhunnatham, P.; Karakalos, S. G.; Smith, M. D.; Greytak, A. B.; Garashchuk, S.; Shustova, N. B. Connecting Wires: Photoinduced Electronic Structure Modulation in Metal-Organic Frameworks. *J. Am. Chem. Soc.* **2019**, *141*, 5350−5358.
(66) Seiler, V. K.; Robeyns, K.; Tumanov, N.; Cinčić, D.; Wouters, J.; Champagne, B.; Leyssens, T. A Coloring Tool for Spiropyrans: Solid State Metal-Organic Complexation versus Salification. *CrystEngComm* **2019**, *21*, 4925−4933.
(67) Feuerstein, T. J.; Müller, R.; Barner-Kowollik, C.; Roesky, P. W. Investigating the Photochemistry of Spiropyran Metal Complexes with Online LED-NMR. *Inorg. Chem.* **2019**, *58*, 15479−15486.
(68) Rostovtseva, I. A.; Chernyshev, A. V.; Tkachev, V. V.; Dorogan, I. V.; Voloshin, N. A.; Solov'eva, E. V.; Metelitsa, A. V.; Gaeva, E. B.; Aldoshin, S. M.; Minkin, V. I. Experimental and Theoretical Insight into the Complexation Behavior of Spironaphthopyrans Bearing *o*-Positioning Benzazole Moiety. *J. Mol. Struct.* **2017**, *1145*, 55−64.
(69) Remacle, F.; Speiser, S.; Levine, R. D. Intermolecular and Intramolecular Logic Gates. *J. Phys. Chem. B* **2001**, *105*, 5589−5591.
(70) Nordin, R.; Lazim, A. M.; Hasbullah, S. A. Spectral and Photochromic Study of Spiropyran. *AIP Conf. Proc.* **2013**, *1571*, 817.
(71) Natali, M.; Giordani, S. Interaction Studies between Photochromic Spiropyrans and Transition Metal Cations: The Curious Case of Copper. *Org. Biomol. Chem.* **2012**, *10*, 1162−1171.
(72) Martin, C. R.; Leith, G. A.; Kittikhunnatham, P.; Park, K. C.; Ejegbavwo, O. A.; Mathur, A.; Callahan, C. R.; Desmond, S. L.; Keener, M. R.; Ahmed, F.; Pandey, S.; Smith, M. D.; Phillpot, S. R.; Greytak, A. B.; Shustova, N. B. Heterometallic Actinide-Containing Photoresponsive Metal-Organic Frameworks: Dynamic and Static Tuning of Electronic Properties. *Angew. Chem., Int. Ed.* **2021**, *60*, 8072−8080.
(73) Wudl, F.; Bryce, M. R. Apparatus for Two-Probe Conductivity Measurements on Compressed Powders. *J. Chem. Educ.* **1990**, *67*, 717−718.
(74) Sun, L.; Park, S. S.; Sheberla, D.; Dincă, M. Measuring and Reporting Electrical Conductivity in Metal-Organic Frameworks: Cd_2(TTFTB) as a Case Study. *J. Am. Chem. Soc.* **2016**, *138*, 14772−14782.
(75) Šimėnas, M.; Kobalz, M.; Mendt, M.; Eckold, P.; Krautscheid, H.; Banys, J.; Pöppl, A. Synthesis, Structure, and Electron Paramagnetic Resonance Study of a Mixed Valent Metal-Organic Framework Containing Cu_2 Paddle-Wheel Units. *J. Phys. Chem. C* **2015**, *119*, 4898−4907.
(76) Del Sesto, R. E.; Arif, A. M.; Miller, J. S. Copper(II) Benzoate Nitroxide Dimers and Chains: Structure and Magnetic Studies. *Inorg. Chem.* **2000**, *39*, 4894−4902.
(77) Świątkowski, M.; Lanka, S.; Czylkowska, A.; Gas, K.; Sawicki, M. Structural, Spectroscopic, Thermal, and Magnetic Properties of a New Dinuclear Copper Coordination Compound with Tiglic Acid. *Materials* **2021**, *14*, 2148.

https://doi.org/10.1021/jacs.1c11984
J. Am. Chem. Soc. 2022, 144, 4457−4468

(78) Yurtaeva, S. V.; Gilmutdinov, I. F.; Rodionov, A. A.; Zaripov, R. B.; Kutyreva, M. P.; Bondar, O. V.; Nedopekin, O. V.; Khafizov, N. R.; Kadkin, O. N. Ferromagnetically Coupled Copper(II) Clusters Incorporated in Functionalized Boltorn H30 Hyperbranched Polymer Architecture: ESR, Magnetic Susceptibility Measurements, and Quantum-Chemical Calculations. *ACS Omega* **2019**, *4*, 16450−16461.
(79) Gautier-Luneau, I.; Phanon, D.; Duboc, C.; Luneau, D.; Pierre, J. L. Electron Delocalisation in a Trinuclear Copper(II) Complex: High-Field EPR Characterization and Magnetic Properties of $Na_3[Cu_3(mal)_3(H_2O)]\cdot 8H_2O$. *Dalton Trans.* **2005**, 3795−3799.
(80) Paredes-García, V.; Santana, R. C.; Madrid, R.; Vega, A.; Spodine, E.; Venegas-Yazigi, D. Unusual Conformation of a Dinuclear Paddle Wheel Copper(II) Complex. Synthesis, Structural Characterization and EPR Studies. *Inorg. Chem.* **2013**, *52*, 8369−8377.
(81) Ozarowski, A. The Zero-Field-Splitting Parameter D in Binuclear Copper(II) Carboxylates Is Negative. *Inorg. Chem.* **2008**, *47*, 9760−9762.
(82) Alter, M.; Binet, L.; Touati, N.; Lubin-Germain, N.; Le Hô, A. S.; Mirambet, F.; Gourier, D. Photochemical Origin of the Darkening of Copper Acetate and Resinate Pigments in Historical Paintings. *Inorg. Chem.* **2019**, *58*, 13115−13128.
(83) Dolgopolova, E. A.; Brandt, A. J.; Ejegbavwo, O. A.; Duke, A. S.; Maddumapatabandi, T. D.; Galhenage, R. P.; Larson, B. W.; Reid, O. G.; Ammal, S. C.; Heyden, A.; Chandrashekhar, M.; Stavila, V.; Chen, D. A.; Shustova, N. B. Electronic Properties of Bimetallic Metal-Organic Frameworks (MOFs): Tailoring the Density of Electronic States through MOF Modularity. *J. Am. Chem. Soc.* **2017**, *139*, 5201−5209.
(84) Biesinger, M. C. Advanced Analysis of Copper X-Ray Photoelectron Spectra. *Surf. Interface Anal.* **2017**, *49*, 1325−1334.
(85) Ilton, E. S.; Post, J. E.; Heaney, P. J.; Ling, F. T.; Kerisit, S. N. XPS Determination of Mn Oxidation States in Mn (hydr)oxides. *Appl. Surf. Sci.* **2016**, *366*, 475−485.
(86) Duke, A. S.; Dolgopolova, E. A.; Galhenage, R. P.; Ammal, S. C.; Heyden, A.; Smith, M. D.; Chen, D. A.; Shustova, N. B. Active Sites in Copper-Based Metal-Organic Frameworks: Understanding Substrate Dynamics, Redox Processes, and Valence-Band Structure. *J. Phys. Chem. C* **2015**, *119*, 27457−27466.
(87) Ilton, E. S.; Du, Y.; Stubbs, J. E.; Eng, P. J.; Chaka, A. M.; Bargar, J. R.; Nelin, C. J.; Bagus, P. S. Quantifying Small Changes in Uranium Oxidation States Using XPS of a Shallow Core Level. *Phys. Chem. Chem. Phys.* **2017**, *19*, 30473−30480.
(88) Armendáriz-Vidales, G.; Martínez-González, E.; Hernández-Melo, D.; Tiburcio, J.; Frontana, C. Electrochemical Characterization of Spiropyran Structures. *Procedia Chem.* **2014**, *12*, 41−46.
(89) Bobo, M. V.; Arcidiacono, A. M.; Ayare, P. J.; Reed, J. C.; Helton, M. R.; Ngo, T.; Hanson, K.; Vannucci, A. K. A Series of Green Light Absorbing Organic Photosensitizers Capable of Oxidative Quenching Photocatalysis. *ChemPhotoChem.* **2021**, *5*, 51−57.
(90) Joshi-Pangu, A.; Lévesque, F.; Roth, H. G.; Oliver, S. F.; Campeau, L. C.; Nicewicz, D.; DiRocco, D. A. Acridinium-Based Photocatalysts: A Sustainable Option in Photoredox Catalysis. *J. Org. Chem.* **2016**, *81*, 7244−7249.
(91) Singha, N. K.; German, A. L. Atom Transfer Radical Polymerization of Styrene Using a Copper Catalyst with a Pseudohalogen Anion. *J. Appl. Polym. Sci.* **2005**, *98*, 1418−1426.
(92) Scott, M. J.; Billiar, T. R.; Stoyanovsky, D. A. N-*tert*-butylmethanimine N-Oxide Is an Efficient Spin-Trapping Probe for EPR Analysis of Glutathione Thiyl Radical. *Sci. Reports* **2016**, *6*, 38773.
(93) Ranguelova, K.; Mason, R. P. The Fidelity of Spin Trapping with DMPO in Biological Systems. *Magn. Reson. Chem.* **2011**, *49*, 152−158.
(94) Buettner, G. R. The Spin Trapping of Superoxide and Hydroxyl Free Radicals with DMPO (5,5-dimethylpyrroline-N-oxide): more about iron. *Free Radic. Res. Commun.* **1993**, *19*, S79−S87.
(95) Karoui, H.; Hogg, N.; Fréjaville, C.; Tordo, P.; Kalyanaraman, B. Characterization of Sulfur-Centered Radical Intermediates Formed during the Oxidation of Thiols and Sulfite by Peroxynitrite: ESR-SPIN Trapping and Oxygen Uptake Studies. *J. Biol. Chem.* **1996**, *271*, 6000−6009.
(96) Zamora, P. L.; Villamena, F. A. Theoretical and Experimental Studies of the Spin Trapping of Inorganic Radicals by 5,5-Dimethyl-1-Pyrroline N-Oxide (DMPO). 3. Sulfur Dioxide, Sulfite, and Sulfate Radical Anions. *J. Phys. Chem. A* **2012**, *116*, 7210−7218.
(97) Li, L.; Abe, Y.; Kanagawa, K.; Usui, N.; Imai, K.; Mashino, T.; Mochizuki, M.; Miyata, N. Distinguishing the 5,5-Dimethyl-1-Pyrroline N-Oxide (DMPO)-OH Radical Quenching Effect from the Hydroxyl Radical Scavenging Effect in the ESR Spin-Trapping Method. *Anal. Chim. Acta* **2004**, *512*, 121−124.
(98) Singh, R. J.; Karoui, H.; Gunther, M. R.; Beckman, J. S.; Mason, R. P.; Kalyanaraman, B. Reexamination of the Mechanism of Hydroxyl Radical Adducts Formed from the Reaction between Familial Amyotrophic Lateral Sclerosis-Associated Cu,Zn Superoxide Dismutase Mutants and H_2O_2. *Proc. Natl. Acad. Sci. U. S. A.* **1998**, *95*, 6675−6680.
(99) Jones, C. M.; Burkitt, M. J. EPR Detection of the Unstable Tert-Butylperoxyl Radical Adduct of the Spin Trap 5,5-Dimethyl-1-Pyrroline N-Oxide: A Combined Spin-Trapping and Continuous-Flow Investigation. *J. Chem. Soc., Perkin Trans.* **2002**, *2*, 2044−2051.
(100) Clément, J. L.; Ferré, N.; Siri, D.; Karoui, H.; Rockenbauer, A.; Tordo, P. Assignment of the EPR Spectrum of 5,5-Dimethyl-1-Pyrroline N-Oxide (DMPO) Superoxide Spin Adduct. *J. Org. Chem.* **2005**, *70*, 1198−1203.
(101) Zhang, Z.-X.; Wei, W.; Bai, F.-Q.; Bibi, S.; Zhang, H.-X. The Phosphorescence Properties of a Series of Diarylethene-Containing Platinum Complexes: The Effect of Ligand Photoisomerization. *Org. Chem. Front.* **2017**, *4*, 2191−2201.
(102) Stranius, K.; Börjesson, K. Determining the Photoisomerization Quantum Yield of Photoswitchable Molecules in Solution and in the Solid State. *Sci. Rep.* **2017**, *7*, 41145.
(103) Samai, S.; Bradley, D. J.; Choi, T. L. Y.; Yan, Y.; Ginger, D. S. Temperature-Dependent Photoisomerization Quantum Yields for Azobenzene-Modified DNA. *J. Phys. Chem. C* **2017**, *121*, 6997−7004.
(104) Shinoda, K.; Yokojima, S.; Fukaminato, T.; Nakamura, S. Determining Factor of the Quantum Yield of the Cyclization Reaction via Triplet States for Dye-Attached Diarylethene. *J. Phys. Chem. A* **2021**, *125*, 5895−5902.
(105) Morimitsu, K.; Kobatake, S.; Irie, M. Control of Cycloreversion Quantum Yields of Diarylethenes by Introduction of Substituents at the Reactive Carbons. *Mol. Cryst. Liq. Cryst.* **2005**, *431*, 451−454.
(106) Shibata, K.; Muto, K.; Kobatake, S.; Irie, M. Photocyclization/Cycloreversion Quantum Yields of Diarylethenes in Single Crystals. *J. Phys. Chem. A* **2002**, *106*, 209−214.
(107) Li, W.; Li, X.; Xie, Y.; Wu, Y.; Li, M.; Wu, X. Y.; Zhu, W. H.; Tian, H. Enantiospecific Photoresponse of Sterically Hindered Diarylethenes for Chiroptical Switches and Photomemories. *Sci. Reports* **2015**, *5*, 9186.
(108) Qin, Y.; Wang, Y.-T.; Yang, H.-B.; Zhu, W. Recent Advances on the Construction of Diarylethene-Based Supramolecular Metallacycles and Metallacages via Coordination-Driven Self-Assembly. *Chem. Synth.* **2021**, *1*, 2.
(109) Frigoli, M.; Mehl, G. H. The Enhancement of Photoswitching in a Diarylethene Derivative by the Incorporation of Cyanobiphenyl Groups. *Chem. Commun.* **2004**, 818−819.
(110) Cox, J. M.; Walton, I. M.; Benedict, J. B. On the Design of Atropisomer-Separable Photochromic Diarylethene-Based Metal−Organic Framework Linkers. *J. Mater. Chem. C* **2016**, *4*, 4028−4033.
(111) Uchida, K.; Nakayama, Y.; Irie, M. Thermally Irreversible Photochromic Systems. Reversible Photocyclization of 1,2-Bis(benzo[*b*]thiophen-3-yl)ethene Derivatives. *Bull. Chem. Soc. Jpn.* **1990**, *63*, 1311−1315.
(112) Irie, M.; Miyatake, O.; Uchida, K. Blocked Photochromism of Diarylethenes. *J. Am. Chem. Soc.* **1992**, *114*, 8715−8716.

https://doi.org/10.1021/jacs.1c11984
J. Am. Chem. Soc. 2022, 144, 4457−4468

(113) Takeshita, M.; Tanaka, C.; Miyazaki, T.; Fukushima, Y.; Nagai, M. Synthesis and Photochromic Properties of Thiophenophan-1-enes Containing a Polyether Bridge. *New J. Chem.* **2009**, *33*, 1433−1438.
(114) Takeshita, M.; Kato, N.; Kawauchi, S.; Imase, T.; Watanabe, J.; Irie, M. Photochromism of Dithienylethenes Included in Cyclodextrins. *J. Org. Chem.* **1998**, *63*, 9306−9313.
(115) Kaieda, T.; Kobatake, S.; Miyasaka, H.; Murakami, M.; Iwai, N.; Nagata, Y.; Itaya, A.; Irie, M. Efficient Photocyclization of Dithienylethene Dimer, Trimer, and Tetramer: Quantum Yield and Reaction Dynamics. *J. Am. Chem. Soc.* **2002**, *124*, 2015−2024.
(116) Irie, M. Diarylethenes for Memories and Switches. *Chem. Rev.* **2000**, *100*, 1685−1716.
(117) Zhang, Y.-H.; Sun, X.-W.; Zhang, T.-S.; Liu, X.-Y.; Cui, G. Nonadiabatic Dynamics Simulations on Early-Time Photochemistry of Spirobenzopyran. *J. Phys. Chem. A* **2020**, *124*, 2547−2559.
(118) Fidder, H.; Rini, M.; Nibbering, E. T. J. The Role of Large Conformational Changes in Efficient Ultrafast Internal Conversion: Deviations from the Energy Gap Law. *J. Am. Chem. Soc.* **2004**, *126*, 3789−3794.
(119) Vázquez, A.; Nudelman, N. S. Photokinetics of Two Novel Photochromic Diarylethenes Derived from Benzothiophene. *Int. J. Chem. Kinet.* **2012**, *44*, 736−744.
(120) Cui, S.; Yang, Y.; Pu, S. Reaction Kinetics and Optical Storage Characters of a New Diarylethene Materials with Composite Properties. *Adv. Mater. Res.* **2012**, *583*, 105−108.
(121) Li, M.; Pu, S.; Zheng, C.; Luo, M.; Le, Z. Photochromic Kinetics of Asymmetrical Diarylethenes in Different Solvents and in PMMA Films. *Surf. Rev. Lett.* **2008**, *15*, 145−151.
(122) Zanoni, M.; Coleman, S.; Fraser, K. J.; Byrne, R.; Wagner, K.; Gambhir, S.; Officer, D. L.; Wallace, G. G.; Diamond, D. Physicochemical Study of Spiropyran−Terthiophene Derivatives: Photochemistry and Thermodynamics. *Phys. Chem. Chem. Phys.* **2012**, *14*, 9112−9120.
(123) Stafforst, T.; Hilvert, D. Kinetic Characterization of Spiropyrans in Aqueous Media. *Chem. Commun.* **2009**, 287−288.
(124) Rini, M.; Holm, A. K.; Nibbering, E. T. J.; Fidder, H. Ultrafast UV-Mid-IR Investigation of the Ring Opening Reaction of a Photochromic Spiropyran. *J. Am. Chem. Soc.* **2003**, *125*, 3028−3034.
(125) Buback, J.; Kullmann, M.; Langhojer, F.; Nuernberger, P.; Schmidt, R.; Würthner, F.; Brixner, T. Ultrafast Bidirectional Photoswitching of a Spiropyran. *J. Am. Chem. Soc.* **2010**, *132*, 16510−16519.
(126) Kortekaas, L.; Chen, J.; Jacquemin, D.; Browne, W. R. Proton-Stabilized Photochemically Reversible *E*/*Z* Isomerization of Spiropyrans. *J. Phys. Chem. B* **2018**, *122*, 6423−6430.

https://doi.org/10.1021/jacs.1c11984
J. Am. Chem. Soc. 2022, 144, 4457−4468